Validation of full-wave simulations for mode conversion of waves in the ion cyclotron range of frequencies with phase contrast imaging in Alcator C-Mod

Citation: Tsujii, N. et al. "Validation of Full-Wave Simulations for Mode Conversion of Waves in the Ion Cyclotron Range of Frequencies with Phase Contrast Imaging in Alcator C-Mod." Physics of Plasmas 22.8 (2015): 082502.

As Published: http://dx.doi.org/10.1063/1.4927912

Publisher: American Institute of Physics (AIP)

Persistent URL: http://hdl.handle.net/1721.1/108416

Version: Original manuscript: author's manuscript prior to formal peer review

PSFC/JA-15-27

Validation of Full-Wave Simulations for Mode Conversion of Waves in the Ion Cyclotron Range of Frequencies with Phase Contrast Imaging in Alcator C-Mod

[1]Tsujii, N., [2]Porkolab, M., [2]Bonoli, P.T., [2]Edlund, E.,
[2]Ennever, P.C., [2]Lin, Y., [2]Wright, J.C., [2]Wukitch, S.J.,
[3]Jaeger, E.F., [4]Green, D.L., and [5]Harvey, R.W.

[1] Graduate School of Frontier Sciences, University of Tokyo, Chiba 277-8561, Japan
[2] MIT Plasma Science and Fusion Center, Cambridge, MA 02139 USA
[3] XCEL Engineering, Inc., Oak Ridge, TN 37830 USA
[4] Oak Ridge National Laboratory, Oak Ridge, TN 37831 USA
[5] CompX, Del Mar, CA 92014 USA

May 2015

Plasma Science and Fusion Center
Massachusetts Institute of Technology
Cambridge MA 02139 USA

This work was supported by the U.S. Department of Energy, Grant No. DE-FG02-94ER54235.

Validation of full-wave simulations for mode conversion of waves in the ion cyclotron range of frequencies with phase contrast imaging in Alcator C-Mod

N. Tsujii,[1, a)] M. Porkolab,[2] P. T. Bonoli,[2] E. M. Edlund,[2] P. C. Ennever,[2] Y. Lin,[2] J. C. Wright,[2] S. J. Wukitch,[2] E. F. Jaeger,[3] D. L. Green,[4] and R. W. Harvey[5]

[1)] *Graduate School of Frontier Sciences, The University of Tokyo, Chiba 277-8561, Japan*

[2)] *MIT Plasma Science and Fusion Center, Cambridge, Massachusetts 02139, USA*

[3)] *XCEL Engineering, Inc., Oak Ridge, Tennessee 37830, USA*

[4)] *Oak Ridge National Laboratory, Oak Ridge, Tennessee 37831, USA*

[5)] *CompX, Del Mar, California 92014, USA*

(Dated: 18 May 2015)

Mode conversion of fast waves in the ion cyclotron range of frequencies (ICRF) is known to result in current drive and flow drive under optimised conditions, which may be utilized to control plasma profiles and improve fusion plasma performance. To describe these processes accurately in a realistic toroidal geometry, numerical simulations are essential. Quantitative comparison of these simulations and the actual experimental measurements is important to validate their predictions and to evaluate their limitations. In this study, the phase contrast imaging (PCI) diagnostic was used to directly detect the ICRF waves in the Alcator C-Mod tokamak. The measurements were compared with full-wave simulations through a synthetic diagnostic technique. In this study, mode converted waves in D-^{3}He and D-H plasmas with various ion species compositions were analyzed. For the minority heating cases, self-consistent electric fields and a minority ion distribution function was simulated by iterating a full-wave code and a Fokker-Planck code. The simulated mode converted wave intensity was in excellent agreement with the measurements close to the antenna, but discrepancies remain for comparison at larger distances.

I. INTRODUCTION

Waves in the ion cyclotron range of frequencies (ICRF) are one of the major tools to heat a fusion plasma. RF technology is already available for a long pulse operation (a few tens of minutes) in the relevant frequency range[1]. ICRF heating also works robustly since there is no upper limit in the plasma density for core accessibility. Usually, fast waves are launched from the antenna, and absorbed through various mechanisms depending on the ion species compositions and concentrations. The so called minority heating[2,3] is used most widely, where the fast waves are absorbed by a small fraction of hydrogen ions in a deuterium or helium(-4) plasma.

When two ion species in the plasma have comparable concentrations, mode conversion to slow waves such as ion cyclotron waves (ICWs) and ion Bernstein waves (IBWs) occurs at the two-ion hybrid resonance that exists between the ion cyclotron resonances[4,5]. These slow waves are absorbed relatively strongly, and localized heating occurs around the resonance. The efficiency of mode conversion depends on the location of the two-ion hybrid resonance with respect to the cyclotron resonances, which is determined by the relative ion species concentrations.

Mode conversion is of interest due to appreciable current[6–8] and flow[9–11] that may be driven by the mode converted slow waves. Mode conversion current drive and flow drive open the possibility for ICRF waves to be used as actuators to control plasma profiles and improve fusion plasma performance. Mode conversion current drive is observed under conditions where mode conversion electron heating is dominant. Its impact on the sawtooth instability was investigated on Alcator C-Mod[8]. Full-wave simulation was performed to estimate the rf driven current profile, which was found to be in qualitative agreement with the observed change in the sawtooth period. Mode conversion flow drive has also been investigated on TFTR[9], Alcator C-Mod[10], and JET[11]. The condition for efficient mode conversion ion heating was found to be optimal for flow drive in a D-^{3}He plasma. However, the driven flow in Alcator C-Mod and JET was in the opposite direction. This may partially be explained by direct rf torque input[11,12], but the physics of net flow generation is still not well understood.

Full-wave simulation codes play a crucial role in these studies, since the wave fields simulated by these codes are the basis for all quantitative analyses. For a numerical simulation code to be used as a reliable predictive tool, it is essential that the code be validated against actual experimental measurements. RF wave measurements are especially valuable, since accuracy of the predicted wave field can be tested in detail. Measurements of mode converted IBWs have been performed on Microtor[13,14], TFR[15], ACT-1[16], TNT-A[17], and JIPPT-IIU[18]. Theoretical prediction of the IBW dispersion relation was verified in these experiments. Realistic global full-wave analysis of mode converted waves was first performed at

[a)] tsujii@k.u-tokyo.ac.jp

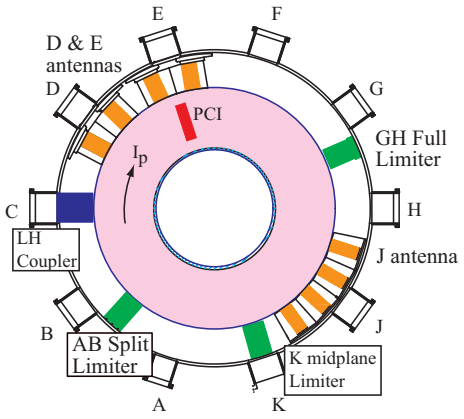

FIG. 1. The top view of the Alcator C-Mod tokamak. The ICRF antennas are located at D, E, and J-port. PCI is located in front of E-antenna.

Alcator C-Mod using a phase contrast imaging (PCI) diagnostic[19]. The measurements were compared with full-wave simulations for different plasma compositions and found to be qualitatively consistent[20,21]. However, the measured absolute wave intensity was significantly weaker than what were simulated[21].

The frequency response of the PCI detector array on Alcator C-Mod was recently recalibrated, and found to be different from the manufacturer's specification (Appendix A). In this study, the ICRF mode conversion experiments on Alcator C-Mod was analyzed once more with the recalibrated PCI measurements. For the minority heating scenario where the deformation of the minority ion distribution function is significant, the full-wave simulation was iterated with a Fokker-Planck simulation to evaluate the electric fields and the minority ion distribution function self-consistently. The absolute intensity of the mode converted waves measured by PCI was compared with the full-wave simulations through a synthetic diagnostic technique for quantitative validation of the simulations.

The organization of this paper is as follows. The experimental setup is described in Sec. II. The numerical simulations used in this study and the synthetic diagnostic technique are described in Sec. III. Quantitative analyses of scenarios with substantial mode conversion are presented in Sec. IV. Analyses of hydrogen minority heating experiments are presented in Sec. V. The results are discussed further in Sec. VI. Conclusions and future work are given in Sec. VII.

II. EXPERIMENTAL SETUP

Alcator C-Mod is a compact ($R = 0.67$ m), high field ($B_\phi < 8$ T) tokamak with a diverted geometry[22]. The machine is equipped with three ICRF antennas. The toroidal locations of the antennas are shown in Fig. 1. Two-strap dipole antennas at D and E-port are operated at 80.5 and 80.0 MHz, respectively, and have 2 MW of source power each[23]. A four-strap antenna with variable phasing at J-port is operated at 50.0-78.0 MHz, and has 4 MW of source power[24]. For the experiments presented in this paper, J-antenna could be phased at 180° or "symmetric" phasing ($[0°, 180°, 180°, 0°]$), +90° phasing ($[0°, 90°, 180°, 270°]$), and -90° phasing ($[0°, -90°, -180°, -270°]$). Typically, cyclotron heating of minority hydrogen ions (minority heating) is performed with the ∼80 MHz systems at 5.2 T. D-^{3}He mode conversion heating can be performed at the same toroidal field by operating J-antenna at 50 MHz.

The rf waves were measured using a phase contrast imaging (PCI) diagnostic[25]. PCI is a type of an interferometer, which measures the phase delay $\tilde{\phi}(x)$ introduced to the laser beam by electron density fluctuations

$$\tilde{\phi}(x) \simeq -r_e \lambda_0 \int dz\, \tilde{n}_e(x, z), \tag{1}$$

where $r_e = e^2/4\pi\epsilon_0 m_e c^2$ is the classical electron radius, λ_0 (=10.6 μm for a CO_2 laser) is the laser wavelength, and z is the distance along the beam chords. The diagnostic has a low wavenumber cutoff, and cannot be used to measure the bulk density profile, but it is designed to be optimal for fluctuation measurements. Optical heterodyne technique was used to down-shift the signal frequency to within a detectable range[19]. The detector frequency bandwidth is 230 kHz (Appendix A). The sightline is vertical and radial image of the line-integrated density fluctuations are measured with a one-dimensional detector array. The PCI diagnostic is located at E-port (Fig. 1) and the wave field can be measured at toroidal angles of 0° (E-antanna), 36° (D-antenna), and -144° (J-antenna) with respect to the antenna. In this study, the low wavenumber cutoff was set to 1.5 cm^{-1}. As a result, the fast wave fluctuations were filtered out, and only the mode converted waves were detected.

III. NUMERICAL SIMULATIONS

Two different simulation codes AORSA[26] and TORIC[27] were used to model the ICRF waves. Both codes are two-dimensional full-wave solvers for rf waves in an axisymmetric plasma. AORSA uses a spectral representation of the wave electric fields and valid to all-orders in Larmor radius and for arbitrary number of cyclotron harmonics[26]. AORSA is also coupled to a Fokker-Planck code CQL3D[28] for self-consistent simulation of electric fields and distribution functions[29].

TORIC uses a finite Larmor radius expansion of the wave equation[27], but is expected to give sufficiently accurate predictions of mode conversion for various heating scenarios such as those presented in this work. The electric field representation is spectral in the poloidal direction and finite element in the radial direction. Usage of the finite element method substantially reduces the computational resource required for TORIC to less than

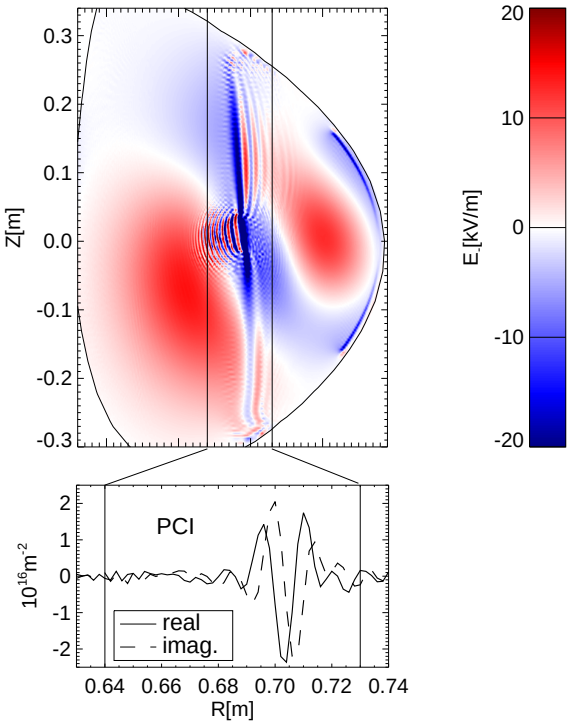

FIG. 2. The left-hand circularly polarized component of the electric field simulated by AORSA (top) and the simulated PCI signal (bottom) in a D-^{3}He plasma, 1 MW rf power. Reprinted with permission from[21]. Copyright 2012 American Institute of Physics.

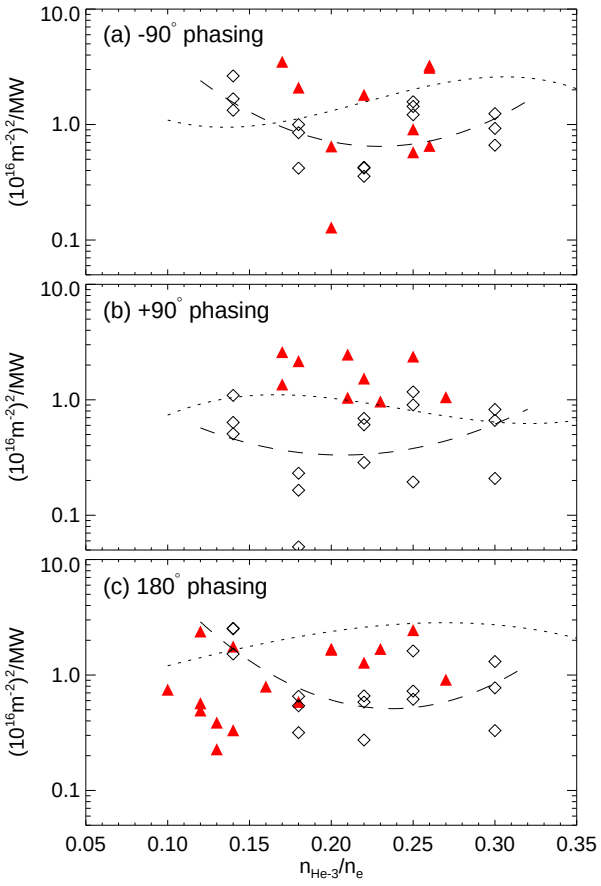

FIG. 3. The measured PCI signal intensity per unit launched rf power (red triangles) and the AORSA prediction (black diamonds) versus the helium-3 concentration at (a) -90° (b) +90° (c) 180° antenna phasing. The dashed curves show the fit to the AORSA predictions. The dotted curves show the fit to the TORIC predictions (data points not shown for brevity).

a hundredth of that for AORSA. Since much less computationally expensive, TORIC has been very useful to perform a large number of parameter scans.

The predictions were compared to PCI measurements through a synthetic diagnostic technique. The electron density fluctuations of the rf waves $\tilde{n}_e$ are evaluated from the continuity equation

$$\tilde{n}_e = \frac{i}{e\omega}\nabla\cdot(\sigma_e\cdot\tilde{E}), \qquad (2)$$

where σ_e is the dielectric modeled in the full-wave code and $\tilde{E}$ is the electric field solution. The resulting three-dimensional electron density fluctuation profile was integrated along the PCI chords to "synthesize" the PCI signal (Fig. 2). Since the results can be directly compared with the measurements, the technique is ideal for code validation purposes.

IV. ANALYSIS OF THE MODE CONVERSION EXPERIMENTS

When more than two ion species have comparable concentrations, appreciable fraction of power is absorbed in the proximity of the two-ion hybrid resonance through mode conversion. This is a condition favorable for detecting mode converted waves with PCI. The ion distribution functions can be considered Maxwellian in this regime.

A. Antenna phasing dependence in the D-^{3}He mode conversion scenario

On Alcator C-Mod, a D-^{3}He plasma with more than ~13 % helium-3 concentration has an optimum mode conversion efficiency for low-field side launch. J-antenna was operated at 50 MHz to perform D-^{3}He mode conversion heating at ~5 T. The PCI diagnostic is located at toroidal angle $\phi = -144°$ with respect to this antenna. Comparison of the mode converted wave intensity measured by PCI and the full-wave predictions by AORSA and TORIC for various J-antenna phasings are shown in Fig. 3. The absorption efficiency is evaluated from change in the magnetic stored energy during the rf pulse[21]. Maxwellian ion distribution was assumed for all simulations. The measured wave intensity has a weak

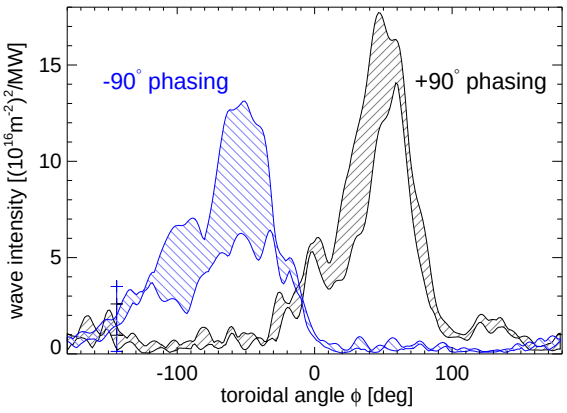

FIG. 4. The toroidal variation of the peak PCI signal intensity simulated by AORSA (per unit launched rf power). Blue hatched area: -90° antenna phasing. Gray hatched area: +90° antenna phasing. Blue plus symbols: range of measured wave intensities for -90° antenna phasing. Gray plus symbols: range of measured wave intensities for +90° antenna phasing.

dependence on the helium-3 concentration in this parameter range, consistent with the full-wave predictions.

The difference between the wave intensity predicted for +90° and -90° phasings can be understood in terms of toroidal direction of the waves launched from the antenna. Figure 4 shows the toroidal variation of the peak PCI signal intensity simulated by AORSA. The plasma parameters for the simulation are $B_{\phi 0} = 5.6$ T, $I_p = 0.81$ MA, $\bar{n}_e = 1.2\times10^{20}$ m^{-3}, and $n_{\text{He-3}}/n_e = 0.22$. The hatched area indicates the range of predicted PCI signal intensity for different PCI beam angles within the uncertainty of beam alignment. The plus symbols show the range of measured wave intensity. The waves propagate short way around the torus with -90° phasing, and the predicted wave intensity tends to be stronger for this phasing.

Good agreement between the measurement and the simulation is obtained for -90° phasing, when the waves are launched towards the measurement location (Fig. 3 (a)). AORSA and TORIC predictions are within a factor of two of each other which is acceptable considering the large scatter in the data points. When the waves are launched long way around the torus (+90°, b), the predicted wave intensity is about a factor of 2 weaker compared to the other direction. The prediction is also weaker than the measurement, but it is expected to be less accurate due to the larger distance the waves need to travel. The comparison for symmetric phasing (c) is reasonable overall, with slight overprediction of the wave intensity at lower helium-3 concentrations. This may be due to interference of the waves propagating in opposite directions that is difficult to simulate exactly. Larger discrepancy between AORSA and TORIC predictions at this phasing may also be related to this uncertainty.

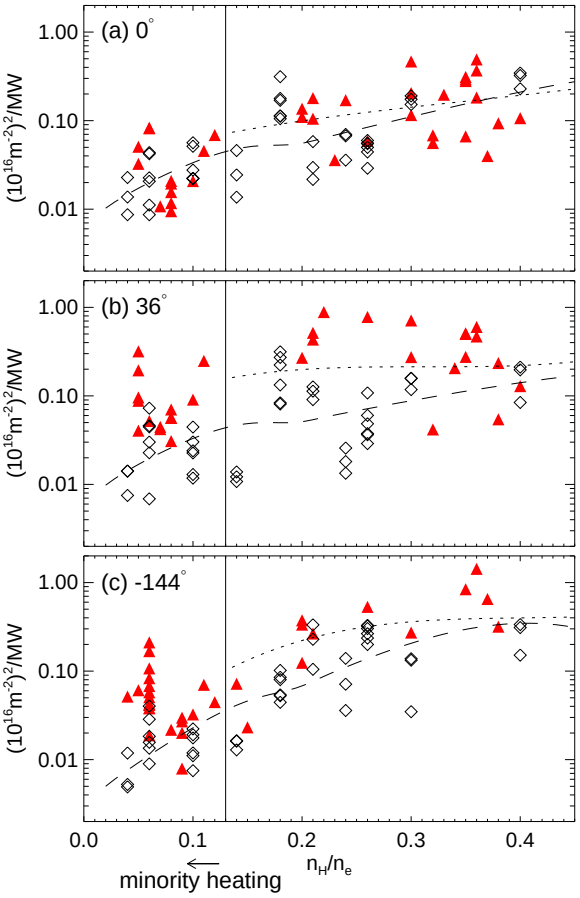

FIG. 5. The measured PCI signal intensity per unit launched rf power (red triangles) and the AORSA prediction (black diamonds) versus the hydrogen concentration at (a) 0° (b) 36° (c) -144° toroidal angle with respect to the antenna. The dashed curves show the fit to the AORSA predictions. The dotted curves show the fit to the TORIC predictions (data points not shown for brevity). Points to the left of the vertical line are in the minority heating regime at 1 MW rf power.

B. Three-dimensional wave field structure in the high H concentration scenario

Mode converted waves in D-H plasmas were measured using antennas operated at three different toroidal locations with respect to the PCI diagnostic. Figure 5 shows the comparison of the mode converted wave intensity measured by PCI and the full-wave predictions at 0° (E-antenna), 36° (D-antenna), and -144° (J-antenna) toroidal angles. AORSA and CQL3D are iterated at 1 MW below $n_{\text{H}}/n_{\text{e}} = 0.13$. Otherwise, Maxwellian distribution is assumed for both AORSA and TORIC. We will focus on the high hydrogen concentration cases in this section. The minority heating cases ($n_{\text{H}}/n_{\text{e}} < 0.1$) will be discussed in Sec. V. It should be noted that the mode converted wave intensity is much smaller in D-H plasmas compared to D-^{3}He plasmas (cf. Fig. 4). The single-pass mode conversion fraction is only a few per-

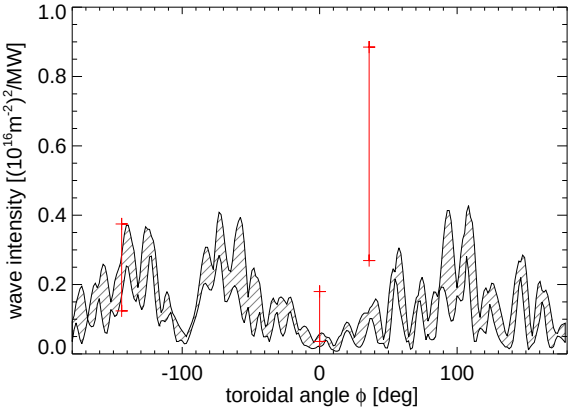

FIG. 6. The toroidal variation of the peak PCI signal intensity simulated by AORSA (per unit launched rf power). $n_{\rm H}/n_{\rm e} = 0.21$, (absorption efficiency) = 0.4. Hatched area: simulation. Red symbols: range of measured wave intensities at $n_{\rm H}/n_{\rm e} = 0.20$-$0.24$.

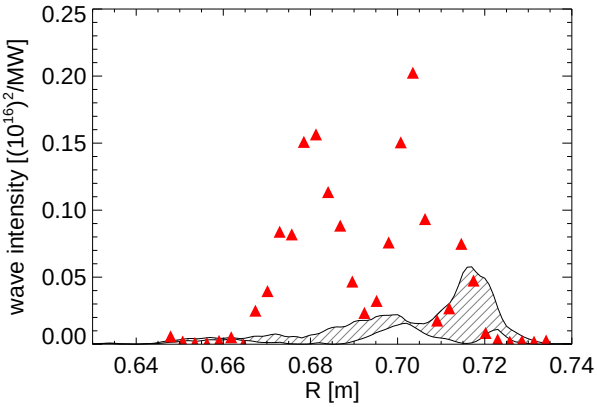

FIG. 7. The radial structure of the measured and the simulated PCI signal intensity per unit launched rf power in front of the antenna (E-antenna). $n_{\rm H}/n_{\rm e} = 0.21$, (absorption efficiency) = 0.4, simulation by AORSA. Gray hatched area: simulation. Red triangles: measurements.

cent in high hydrogen concentration plasmas whereas it is optimum in D-^{3}He plasmas, and the two scenarios have very different heating properties.

The agreement between the simulations and the measurements are excellent in front of the antenna (Fig. 5 (a)). AORSA and TORIC predictions are also within a factor two of each other. The predicted wave intensity is expected to be most accurate at this location, and the agreement observed here is a good validation of the mode conversion physics implemented in these codes. However, at toroidal angle $\phi = 36°$ the wave intensities are likely underpredicted (b). At $\phi = -144°$, the measured wave intensity is somewhat underpredicted with AORSA, although it agrees well with TORIC. Discrepancy between AORSA and TORIC predictions is large at these two toroidal angles. Differences exist in how the two codes model the plasma outside the last-closed flux surface and the antenna. The prediction at large distance from the antenna may be sensitive to these edge modeling, which makes quantitative comparison with experiments very difficult at these locations.

In order to see if small changes in the global wave field structure can explain the discrepancy, the toroidal variation of the peak PCI signal intensity simulated by AORSA is shown in Fig. 6. The plasma parameters are $B_{\phi 0} = 6.0$ T, $I_p = 0.81$ MA, $\bar{n}_e = 1.2 \times 10^{20}$ m^{-3}, and $n_{\rm H}/n_{\rm e} = 0.21$. The hatched area shows the range of predictions for different PCI beam angles as in Fig. 4. The red symbols show the range of the measured PCI signal intensities. The mode converted wave intensity tends to be weak in the vicinity of the antenna ($\phi = 0°$). This is likely due to the higher mode conversion efficiency of waves with higher $k_\parallel \simeq k_\phi$, which propagate to larger toroidal angle. This trend is consistent with the measurements.

Since all these experiments were performed with symmetric antenna phasing, there is an interference pattern due to waves propagating clockwise and counterclockwise toroidally. The resulting peaks and troughs within a small toroidal angle makes a one-to-one comparison of the measurement and the simulation very difficult. However, even taking into account this uncertainty, the intensities at $\phi = 36°$ is appreciably underpredicted with the present model.

For completeness, comparison of the measured and the simulated radial structure of the mode converted waves is shown in Fig. 7. Since the PCI signal is the line-integral of the electron density fluctuations along the beam chords, its exact spatial structure depends sensitively on the detail of the three-dimensional wave field pattern. Therefore, the measured and the simulated PCI signal structure is not expected to agree in every detail. However, the radial extent of the simulated PCI signal agrees well with the measurement, indicating the absorption of the mode converted waves is simulated properly. The measured wave intensity is about a factor of 4 larger than the prediction in this case. The ICW fluctuations around major radius $R = 0.67$–0.71 m have cancelled out as a result of line-integration to produce the PCI signal. The predicted PCI signal here is among the lowest around similar conditions (see Fig. 5 (a), around $n_{\rm H}/n_{\rm e} = 0.21$).

V. ANALYSIS OF HYDROGEN MINORITY HEATING EXPERIMENTS

In the minority heating scenario[2,3], most of the rf power is absorbed by a small fraction of minority ions, and an energetic ion tail forms. The non-thermal ion distribution affects the wave fields and vice versa, and both needs to be solved self-consistently. Heating experiments performed in D-H plasmas for hydrogen concentration

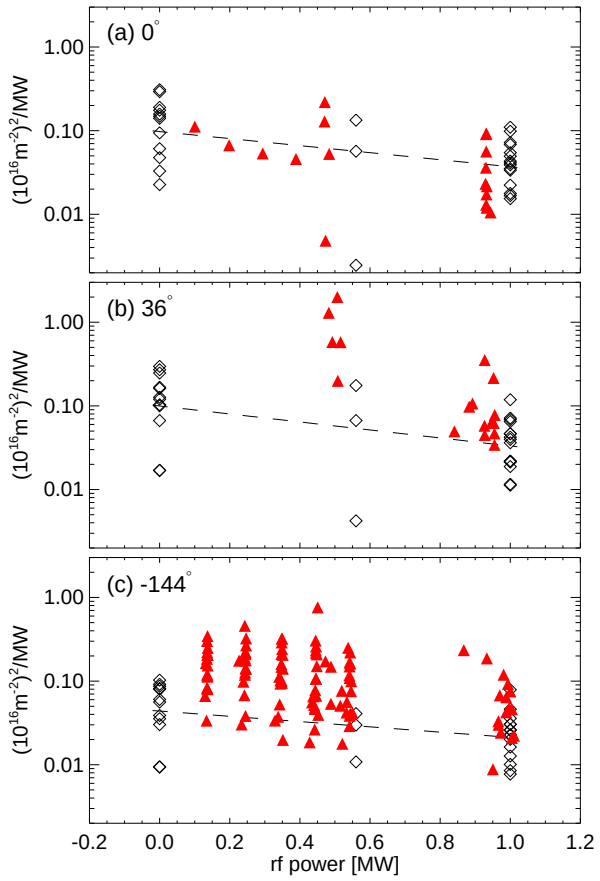

FIG. 8. The measured PCI signal intensity per unit rf power (red triangles) and the AORSA-CQL3D prediction (black diamonds) versus rf power in hydrogen minority heating experiments at (a) 0° (b) 36° (c) -144° toroidal angle with respect to the antenna. The dashed lines are the linear fits to the simulated values. Reprinted with permission from[30]. Copyright 2015 American Institute of Physics.

of 5-10% are analyzed in this section. Although mode conversion is weak under this condition, mode converted waves could still be clearly observed with PCI.

The power dependence of the mode converted wave intensity measured by PCI is shown together with the predictions of the coupled AORSA-CQL3D simulation in Fig. 8. The absorption efficiency is assumed to be 90 % in this analysis. Points at 0 MW rf power correspond to simulations performed with a Maxwellian distribution function. There is about a factor of 2 reduction in the predicted mode converted wave intensity from 0 to 1 MW. The simulation is in excellent agreement with the measurements in front of the antenna ($\phi = 0°$, a). At toroidal angle $\phi = -144°$ (c), the power dependence is reproduced but the predicted overall wave intensity is about a factor of 4 weaker than the measurements. The number of data points for $\phi = 36°$ (b) are too limited to be conclusive, but the wave intensity is likely underpredicted.

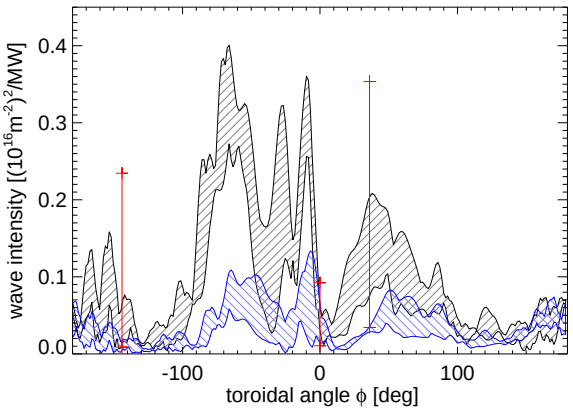

FIG. 9. The toroidal variation of the peak PCI signal intensity simulated by AORSA-CQL3D (per unit rf power). $n_{\rm H}/n_{\rm e} \simeq 0.06$, (rf power) $\simeq 1.0$ MW. Gray hatched area: simulation with Maxwellian hydrogen distribution. Blue hatched area: simulation with non-thermal hydrogen distribution. Red symbols: Range of measured wave intensities.

Again, to see if small changes in the three-dimensional wave field structure can explain the discrepancy, the simulated toroidal variation of the peak PCI signal intensity is shown in Fig. 9. The plasma parameters are $B_{\phi 0} = 5.6$ T, $I_p = 0.81$ MA, and $\bar{n}_e = 1.0 \times 10^{20}$ m^{-3}, $n_{\rm H}/n_{\rm e} = 0.06$, and the rf power is 1 MW. The hatched area shows the range of predictions for different PCI beam angles within the uncertainty of the beam alignment. In the vicinity of the antenna ($\phi = 0°$), the wave intensity is < 0.3 $(10^{16}$ m$^{-2})^2$ for Maxwellian distribution (black hatched area) and < 0.1 $(10^{16}$ m$^{-2})^2$ for the self-consistent solution (blue hatched area). These values agree well with Fig. 8 (a) which shows the predicted wave intensity exactly at $\phi = 0°$, but with slightly different plasma profiles. The consistency between the two analyses indicates that the peak locations of the toroidal signal structure depend sensitively on the small change in the plasma profiles. On the other hand, the predicted mode converted wave intensity is appreciably weaker than the measurements at the other two toroidal angles even considering the possible shifts of the peaks in the toroidal signal structure.

Since the mode converted slow waves are absorbed locally around the two-ion hybrid resonance, the radial structure of the PCI signal is directly correlated with the energetic minority ion population. Comparison of the simulated and the measured radial wave structure is shown in Fig. 10. The gray hatched area shows the mode converted wave structure for the solution with Maxwellian distribution and the blue hatched area shows that for the self-consistent solution. The radial extent of the measurement agrees well with the self-consistent solution obtained for 1 MW. This suggests that the fast ion population and the damping of the locally excited mode converted waves are simulated accurately.

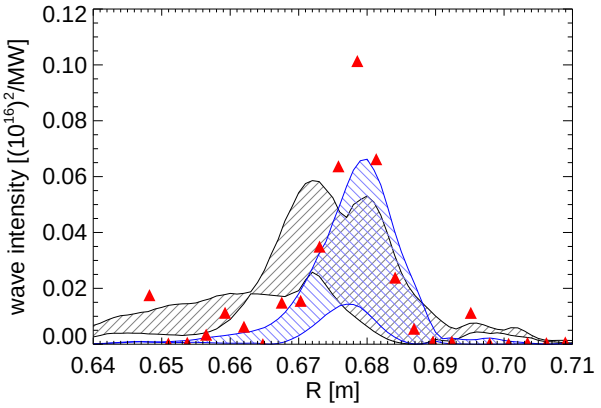

FIG. 10. The radial structure of the measured and the simulated PCI signal intensity per unit rf power at toroidal angle 0° (E-antenna). $n_H/n_e = 0.06$, (rf power) = 1.0 MW, simulation by AORSA-CQL3D. Gray hatched area: simulation with Maxwellian hydrogen distribution. Blue hatched area: simulation with non-thermal hydrogen distribution. Red triangles: measurements.

Discrepancy in the simulated and the measured wave intensity at $\phi = -144°$ (Fig. 8 (c)) is present even at low power levels where deformation of the minority ion distribution function is small. Furthermore, the simulated radial mode converted wave structure at high power (1 MW) agrees well with the measurement. This implies that the problem is not in the simulation of the non-thermal distribution function, but in the three-dimensional wave field structure itself. The wave fields away from the antenna are likely to be inaccurate as it was the case in the mode conversion scenarios presented in the previous section. The presence of the energetic ions may have a smaller impact on the fast wave absorption and the global wave field structure, which may explain the power dependent discrepancy at $\phi = 36°$ (b).

VI. DISCUSSION

The simulated mode converted wave intensity is in excellent agreement with the measurements in front of the antenna (Figs. 5, 8 (a)), where the prediction is expected to be most accurate. However, there still remain some discrepancies at larger toroidal angles from the antenna. Comparison of AORSA and TORIC predictions with matched input profiles is insightful to see the possible inaccuracies. Figures 11 and 12 show the comparison between the two codes for minority heating, and D-H and D-^{3}He mode conversion cases. The minority heating cases are compared for simulations with the Maxwellian distribution function. For all three scenarios, predictions at toroidal angle $\phi = 0°$ (E-antenna) are in good agreement. At the toroidal angles of the other antennas (36°, -144°), however, there is a discrepancy of a factor 2-4.

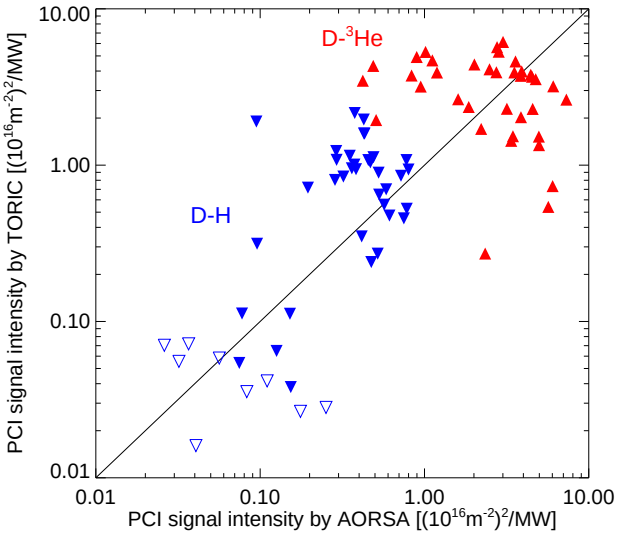

FIG. 11. Comparison of the PCI signal intensity simulated by AORSA and TORIC. Red upward triangles: D-^{3}He plasmas ($n_{He\text{-}3}/n_e$ = 0.16-0.28). Blue downward solid triangles: D-H plasmas (n_H/n_e = 0.20-0.40). Blue downward open triangles: H minority heating (n_H/n_e = 0.04-0.10).

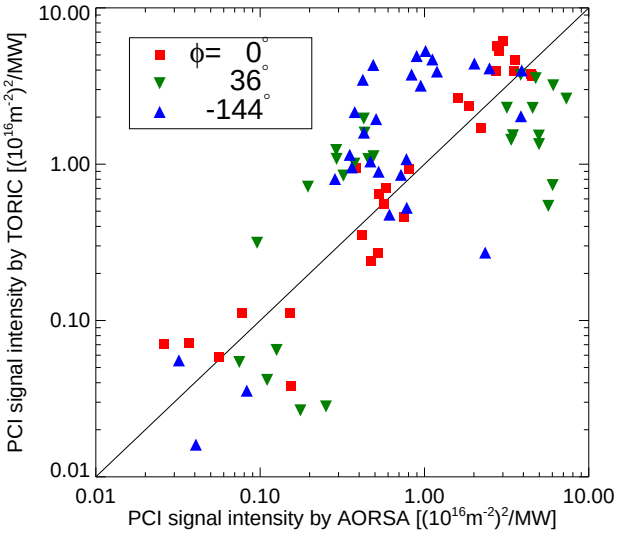

FIG. 12. Comparison of the PCI signal intensity simulated by AORSA and TORIC. Red squares: toroidal angle $\phi = 0°$ (E-antenna). Green downward triangles: 36° (D-antenna). Blue upward triangles: -144° (J-antenna).

AORSA and TORIC have different wave models which may contribute to the discrepancy observed between the two codes. TORIC uses the finite Larmor radius (FLR) approximation of the wave equation whereas AORSA is valid to all-orders. The so-called reduced FLR approximation necessary for numerical reasons[27] is quantitatively accurate for D-H minority heating cases, but is

only qualitatively correct for general strong mode conversion scenarios. However, because of the universality of the mode conversion fraction[5], the impact of this difference to the PCI signal is subtle, if any. Furthermore, considering the fact that the wave intensities predicted by the two codes agree well in front of the antenna, this is not likely to be a serious issue.

Different modeling of plasma edge region between AORSA and TORIC that cannot be matched easily is more likely to be an issue. For AORSA, the antenna was placed a few mm inside the last-closed flux surface (LCFS) and perfectly conducting boundary was assumed at the LCFS for the simulations shown in this paper. For TORIC, the antenna was placed a few mm outside the LCFS and vacuum is assumed between the LCFS and the perfectly conducting wall at a few cm outside the LCFS. In reality, the antennas are about 4 cm outside the LCFS, and the scrape-off-layer (SOL) has a finite plasma density. Somewhat better agreement of the measurements with the TORIC predictions may be due to the similarity of its model to the actual experimental situation.

The plasma edge modeling is important for accurate simulation of the wave coupling from the antenna into the plasma. Flux surface averaged quantities such as the power deposition profiles are determined mostly by the dominant component of the coupled $k_{\|}$ spectrum which can be estimated relatively easily. On the other hand, wave fields at large toroidal angles from the antenna are more sensitive to higher $k_{\|}$ components which do not necessarily contribute substantially to plasma heating. High $k_{\|}$ components are likely to be affected by the larger evanescent gap and, therefore, sensitive to SOL plasma profile. Depending on the phasing, the antenna can also excite $k_{\|}$ not expected from simple rectangular straps due to image currents flowing in the surrounding structure. In this sense, the present antenna model in AORSA and TORIC may be too simplistic. A realistic three-dimensional antenna modeling may be necessary to evaluate the coupled spectrum up to sufficiently high $k_{\|}$ to predict accurately the wave intensities at large toroidal angles from the antenna.

VII. CONCLUSIONS AND FUTURE WORK

The ICRF mode converted waves were measured with a phase contrast imaging (PCI) diagnostic on Alcator C-Mod for mode conversion and minority heating scenarios. Two-dimensional full-wave simulation codes AORSA and TORIC were used to model the ICRF waves. For minority heating scenarios, AORSA was iterated with a Fokker-Planck code CQL3D to obtain self-consistent electric fields and a minority distribution function. The predicted mode converted wave intensity was quantitatively compared to the PCI measurements through a synthetic diagnostic technique.

The simulated mode converted wave intensity in front of the antenna (E-antenna) was in excellent agreement with the measurements for both mode conversion and minority heating cases, which validates the mode conversion physics implemented in the codes to within a factor of 2. On the other hand, at the other toroidal angles of 36° and −144° (D and J-antenna), discrepancy of up to a factor of 4 was observed. AORSA and TORIC predictions also differ by a factor of 2-4 at these toroidal locations. Measurements away from the antenna are sensitive to higher $k_{\|}$ components which may not be simulated accurately with the present simplified model in the plasma edge. Realistic scrape-off-layer and antenna modeling may be necessary to obtain the three-dimensional wave field structure sufficiently accurate for analysis of wave measurements at large toroidal angles from the antenna.

ACKNOWLEDGMENTS

The authors thank the Alcator C-Mod operation and ICRF technical support group. The authors also thank Dr. L. Berry and Dr. C. Phillips for useful discussions over the course of this work. This work used the MIT Plasma Science and Fusion Center Theory Group parallel computational cluster Loki, and computing resources provided through NERSC and the SciDAC Center for Simulation of Wave Plasma Interactions. This work is supported by U.S. Department of Energy under DE-FG02-94-ER54235, DE-FC02-99-ER54512, and DE-FC02-01ER54648.

Appendix A: Frequency response of the PCI detector

The detail of the calibration of the optical system is described in Appendix A of Ref.[21]. The system response was calibrated at 15 kHz and assumed to be flat up to 3 MHz in the paper. At that point, the response time constant of the detectors was thought to be 10 ns, but recent tests of the detector revealed that it was actually only 0.7 μs (0.23 MHz bandwidth). Since the ICRF waves were detected at 0.9-2 MHz, the measured fluctuation amplitudes were underestimated by a factor of 3-8 in the article. Figure 13 shows the test result of the frequency response of the detectors. The frequency response was measured by modulating an LED at known frequencies and amplitudes, and monitoring the detector output. LEDs with 850 nm and 1760 nm wavelengths were used to verify there is no wavelength dependence. The ICRF wave measurements were performed at 0.98 MHz (E-antenna), 0.99, 1.02 MHz (J-antenna), 1.48 MHz (D-antenna) for D-H plasmas, and 2.08 MHz (J-antenna) for D-^{3}He plasmas. In terms of the signal intensity ($\propto$ amplitude^2), systematic error of 10% to 60% is possible from 0.9 to 2 MHz. Together with the uncertainty in the calibration of the optical system response, the net uncertainty in the PCI signal intensity is 40% and 90% (about a factor of two) at 0.9 and 2 MHz, respectively.

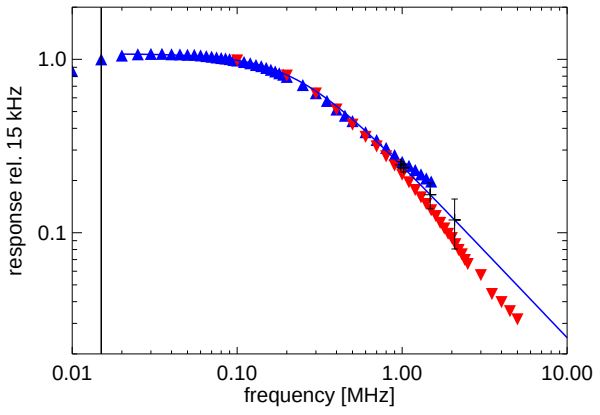

FIG. 13. The detector response versus the signal frequency for the Alcator C-Mod PCI system. The entire optical system is calibrated at 15 kHz (vertical line). The black symbols show the errorbars at the frequencies where the ICRF waves were detected. Blue upward triangles: 850 nm light source. Red downward triangles: 1760 nm light source. Reprinted with permission from[30]. Copyright 2015 American Institute of Physics.

[1]H. Kasahara, T. Seki, K. Saito, R. Seki, R. Kumazawa, Y. Yoshimura, S. Kubo, T. Shimozuma, H. Igami, H. Takahashi, K. Nagasaki, Y. Ueda, M. Tokitani, N. Ashikawa, M. Shoji, T. Wakatsuki, S. Kamio, H. Tsuchiya, S. Yoshimura, N. Tamura, C. Suzuki, H. Yamada, T. Mutoh, and L. E. Group, Physics of Plasmas **21**, 061505 (2014).

[2]T. H. Stix, Nuclear Fusion **15**, 737 (1975).

[3]M. Porkolab, AIP Conference Proceedings **314**, 99 (1994), advances in Plasma Physics Thomas H. Stix Symposium.

[4]F. Perkins, Nuclear Fusion **17**, 1197 (1977).

[5]D. G. Swanson, Physics of Fluids **28**, 2645 (1985).

[6]R. Majeski, J. H. Rogers, S. H. Batha, R. Budny, E. Fredrickson, B. Grek, K. Hill, J. C. Hosea, B. LeBlanc, F. Levinton, M. Murakami, C. K. Phillips, A. T. Ramsey, G. Schilling, G. Taylor, J. R. Wilson, and M. C. Zarnstorff, Phys. Rev. Lett. **76**, 764 (1996).

[7]S. J. Wukitch, Y. Lin, A. Parisot, J. C. Wright, P. T. Bonoli, M. Porkolab, N. Basse, E. Edlund, A. Hubbard, L. Lin, A. Lynn, E. Marmar, D. Mossessian, P. Phillips, and G. Schilling, Physics of Plasmas **12**, 056104 (2005).

[8]A. Parisot, S. J. Wukitch, P. Bonoli, M. Greenwald, A. Hubbard, Y. Lin, R. Parker, M. Porkolab, A. K. Ram, and J. C. Wright, Plasma Physics and Controlled Fusion **49**, 219 (2007).

[9]C. Phillips, M. Bell, R. Bell, S. Bernabei, M. Bettenhausen, C. Bush, D. Clark, D. Darrow, E. Fredrickson, G. Hanson, J. Hosea, B. LeBlanc, R. Majeski, S. Medley, R. Nazikian, M. Ono, H. Park, M. Petrov, J. Rogers, G. Schilling, C. Skinner, D. Smithe, E. Synakowski, G. Taylor, and J. Wilson, Nuclear Fusion **40**, 461 (2000).

[10]Y. Lin, J. Rice, S. Wukitch, M. Reinke, M. Greenwald, A. Hubbard, E. Marmar, Y. Podpaly, M. Porkolab, N. Tsujii, and the Alcator C-Mod team, Nuclear Fusion **51**, 063002 (2011).

[11]Y. Lin, P. Mantica, T. Hellsten, V. Kiptily, E. Lerche, M. F. F. Nave, J. E. Rice, D. V. Eester, P. C. de Vries, R. Felton, C. Giroud, T. Tala, and J. E. Contributors, Plasma Physics and Controlled Fusion **54**, 074001 (2012).

[12]E. F. Jaeger, L. A. Berry, J. R. Myra, D. B. Batchelor, E. D'Azevedo, P. T. Bonoli, C. K. Phillips, D. N. Smithe, D. A. D'Ippolito, M. D. Carter, R. J. Dumont, J. C. Wright, and R. W. Harvey, Phys. Rev. Lett. **90**, 195001 (2003).

[13]P. Lee, R. J. Taylor, W. A. Peebles, H. Park, C. X. Yu, Y. Xu, N. C. Luhmann, and S. X. Jin, Phys. Rev. Lett. **49**, 205 (1982).

[14]H. Park, N. C. Luhmann, W. A. Peebles, and R. Kirkwood, Phys. Rev. Lett. **52**, 1609 (1984).

[15]TFR Group, A. Truc, and D. Gresillon, Nuclear Fusion **22**, 1577 (1982).

[16]G. A. Wurden, M. Ono, and K. L. Wong, Phys. Rev. A **26**, 2297 (1982).

[17]K. Ida, O. Naito, I. Ochiai, S. Shinohara, and K. Miyamoto, Nuclear Fusion **24**, 375 (1984).

[18]T. Tetsuka, K. Kawahata, S. Okajima, A. Nishizawa, T. Watari, R. Ando, S. Tanahashi, K. Toi, and J. Fujita, Journal of the Physical Society of Japan **54**, 3757 (1985).

[19]E. Nelson-Melby, M. Porkolab, P. T. Bonoli, Y. Lin, A. Mazurenko, and S. J. Wukitch, Phys. Rev. Lett. **90**, 155004 (2003).

[20]Y. Lin, S. Wukitch, A. Parisot, J. C. Wright, N. Basse, P. Bonoli, E. Edlund, L. Lin, M. Porkolab, G. Schilling, and P. Phillips, Plasma Physics and Controlled Fusion **47**, 1207 (2005).

[21]N. Tsujii, M. Porkolab, P. T. Bonoli, Y. Lin, J. C. Wright, S. J. Wukitch, E. F. Jaeger, D. L. Green, and R. W. Harvey, Physics of Plasmas **19**, 082508 (2012).

[22]I. H. Hutchinson, R. Boivin, F. Bombarda, P. Bonoli, S. Fairfax, C. Fiore, J. Goetz, S. Golovato, R. Granetz, M. Greenwald, S. Horne, A. Hubbard, J. Irby, B. LaBombard, B. Lipschultz, E. Marmar, G. McCracken, M. Porkolab, J. Rice, J. Snipes, Y. Takase, J. Terry, S. Wolfe, C. Christensen, D. Garnier, M. Graf, T. Hsu, T. Luke, M. May, A. Niemczewski, G. Tinios, J. Schachter, and J. Urbahn, Physics of Plasmas **1**, 1511 (1994).

[23]Y. Takase, S. Golovato, M. Porkolab, K. Bajwa, H. Becker, and D. Caldwell, in *Proceedings of 14th IEEE/NPSS Symposium on Fusion Engineering, San Diego, September 1991* (1991) pp. 118–121 vol.1.

[24]S. J. Wukitch, R. L. Boivin, P. T. Bonoli, J. A. Goetz, J. Irby, I. Hutchinson, Y. Lin, A. Parisot, M. Porkolab, E. Marmar, G. Schilling, and J. R. Wilson, Plasma Physics and Controlled Fusion **46**, 1479 (2004).

[25]M. Porkolab, J. Rost, N. Basse, J. Dorris, E. Edlund, L. Lin, Y. Lin, and S. Wukitch, IEEE Transactions on Plasma Science **34**, 229 (2006), 32nd International Conference on Plasma Science (ICOPS 2005), Monterey, CA, JUN, 2005.

[26]E. F. Jaeger, L. A. Berry, E. F. D'Azevedo, R. F. Barrett, S. D. Ahern, D. W. Swain, D. B. Batchelor, R. W. Harvey, J. R. Myra, D. A. D'Ippolito, C. K. Phillips, E. Valeo, D. N. Smithe, P. T. Bonoli, J. C. Wright, and M. Choi, Physics of Plasmas **15**, 072513 (2008).

[27]M. Brambilla, Plasma Physics and Controlled Fusion **41**, 1 (1999).

[28]R. W. Harvey and M. G. McCoy, in *Proceedings of the IAEA Technical Committee Meeting on Simulation and Modeling of Thermonuclear Plasmas, Montreal, Canada, 1992 (USDOC NTIS Document No. DE93002962)* (1992) p. 40, eDB/700350;.

[29]E. Jaeger, R. Harvey, L. Berry, J. Myra, R. Dumont, C. Phillips, D. Smithe, R. Barrett, D. Batchelor, P. Bonoli, M. Carter, E. D'azevedo, D. D'ippolito, R. Moore, and J. Wright, Nuclear Fusion **46**, S397 (2006).

[30]N. Tsujii, M. Porkolab, P. T. Bonoli, E. M. Edlund, P. C. Ennever, Y. Lin, J. C. Wright, S. J. Wukitch, E. F. Jaeger, D. L. Green, and R. W. Harvey, to be published in AIP Conference Proceedings (2015).